Tunable optical fiber polarization elements based on long-period gratings inscribed in birefringent microstructured fibers

Dimitrios C. Zografopoulos[1,2] and Emmanouil E. Kriezis[1,*]

[1]*Department of Electrical and Computer Engineering, Aristotle University of Thessaloniki, GR-54124, Thessaloniki, Greece*
[2]*E-mail: dzogra@auth.gr*
**Corresponding author: mkriezis@auth.gr*

Received June 8, 2007; revised November 3, 2007; accepted November 6, 2007; posted November 27, 2007 (Doc. ID 83927); published December 21, 2007

The polarization properties of long-period gratings inscribed in highly birefringent photonic crystal fibers are investigated in the context of a multipole method analysis. It is demonstrated that by proper design such fibers may act as selective polarization elements, showing an ample separation of the resonance peaks corresponding to the two orthogonal polarization states. Furthermore, the infiltration of the fiber's capillaries with an isotropic liquid may lead to extensive tuning of the resonant wavelengths. A tuning efficiency of up to 10 nm/°C is demonstrated in the case of a typical infiltrated birefringent photonic crystal fiber. © 2007 Optical Society of America

OCIS codes: 060.2340, 060.2400, 000.4430, 230.5440, 230.3990.

1. INTRODUCTION

Photonic crystal fibers (PCFs) constitute a special type of optical fiber, where light is guided in a defect core formed by locally breaking the symmetry of a periodic microstructured cladding [1]. These fibers have been under intense scientific research during the past years, since their design allows for the sophisticated tailoring of their properties, which may prove indispensable in a wide range of applications [2]. Various PCFs have been demonstrated so far that exhibit remarkable characteristics such as endlessly single-mode operation [3], ultraflattened dispersion [4,5], large mode area [6], and highly nonlinear performance [7]. Furthermore, thermally or electrically tunable operation may also be achieved in PCFs by infiltrating the cladding's capillaries with polymers [8], isotropic liquids [9], or nematic liquid crystalline materials [10–13].

Long-period gratings (LPGs) inscribed in single-mode fibers induce light coupling from the fundamental guided mode to copropagating cladding modes at discrete resonant wavelengths by adding a periodic variation to the refractive index of the fiber core. LPGs have been long used in conventional fibers as band-rejection filters [14], gain-flattening filters for Er-doped fiber amplifiers [15], and polarizing elements [16,17], as well as for spectral shaping [18], dispersion compensation [19], or in numerous sensing applications [20,21]. Moreover, the inscription of LPGs in PCFs (LPG-PCFs) has also been demonstrated by using various techniques, such as UV treatment of a photosensitive Ge-doped fiber core [22], heat treatment with a CO_2 laser [23], an electric arc discharge technique [24], or by applying mechanical pressure [25].

Recently, Wang *et al.* [26] reported an in-fiber polarizer where birefringence in a PCF was induced due to asymmetrical glass ablation and hole collapse during the inscription procedure of a LPG, resulting, thus, in strongly polarization-sensitive losses. In this paper we study numerically the properties of LPGs inscribed in highly birefringent PCFs, under the scope of designing all-fiber polarizing elements for telecommunication applications. It is shown that the values of modal birefringence that may be readily achieved in single-mode LPG-PCFs may lead to significant splitting of the resonance peaks corresponding to the two orthogonal polarization states; thus, undesired phenomena such as polarization mode dispersion may be highly suppressed. In addition, we address the possibility of designing thermally tunable polarizing elements by assessing the infiltration of a birefringent LPG-PCF with an isotropic liquid, whose refractive index value may be adjusted by controlling the operating temperature.

2. STRUCTURAL PARAMETERS AND FIBER DISPERSIVE PROPERTIES

The layout characteristics of the highly birefringent PCF selected for the present study are shown in Fig. 1. The fiber is an index-guided PCF composed of a defect core and a cladding of three rings of cylinders arranged in a triangular lattice, placed in an infinite fiberglass matrix, whose refractive index is denoted n_g. The cylinders are assumed to be either empty ($n_h=1$) or infiltrated with an isotropic liquid. The distance between adjacent cylinders (lattice pitch) is Λ, and the cylinder radius r is set to the value $r=0.2\Lambda$; this value ensures that a photonic crystal with an infinite number of rings in a triangular lattice cladding is endlessly single-mode; i.e., only one guided mode is supported at all wavelengths [27]. In the case here examined, the fiber's cladding is finite; nevertheless, for the wavelength range in the context of the present

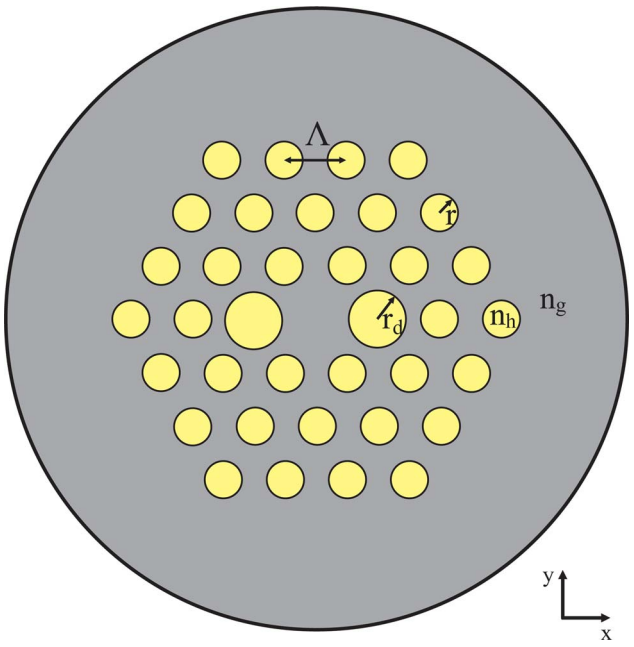

Fig. 1. (Color online) Structural layout of the highly birefringent PCF under study: lattice pitch Λ, capillary radius r, defect radius r_d, and refractive indices of the infinite glass matrix and holes n_g and n_h, respectively.

study the fiber does support only one guided mode [28,29]. In addition, it is known that for PCFs with a finite cladding in an infinite fiberglass matrix, all modes are inherently leaky because of tunneling of optical power from the core into the cladding [30]. Given that, we should clarify that the term "guided" that is used here refers to the modes that are guided in the fiber's core and exhibit strong confinement (in contrast to the significantly more leaky cladding modes) and not to purely lossless modes.

The fiber's symmetry is broken by letting the radius r_d of two cylinders of the first ring around the core obtain values greater than $r_d=0.2\Lambda$. The analysis of the present study will concentrate on the dispersive properties, and the coupling phenomena induced by the LPG inscription, of the fundamental guided mode and the first cladding mode (i.e., the cladding mode with the higher effective index) that belongs to the same class of symmetry [31] as the fundamental mode (hereinafter referred as the target cladding mode). The selection of this particular pair of fundamental cladding modes is based on their coupling efficiency, as will be clarified in Section 3; the analysis for any other pair of modes should follow a similar scheme as well. All calculations have been performed by means of the multipole method [32,33], utilizing a freely available package [34].

As a starting point, we plot in Fig. 2 the dispersion and loss curves of the fundamental and the target cladding mode within a range of normalized frequencies $1<\Lambda/\lambda<3$ for $r_d=r=0.2\Lambda$, for $n_h=1$ and $n_g=1.45$. Owing to the fiber's symmetry, both modes are degenerate: the effective indices for either x- or y-polarized light are identical. The curves corresponding to the confinement loss coefficient (i.e., the imaginary part of the complex modal effective index) show that for $\Lambda/\lambda=3$ the guided mode is very well concentrated in the center, exhibiting a loss coefficient of

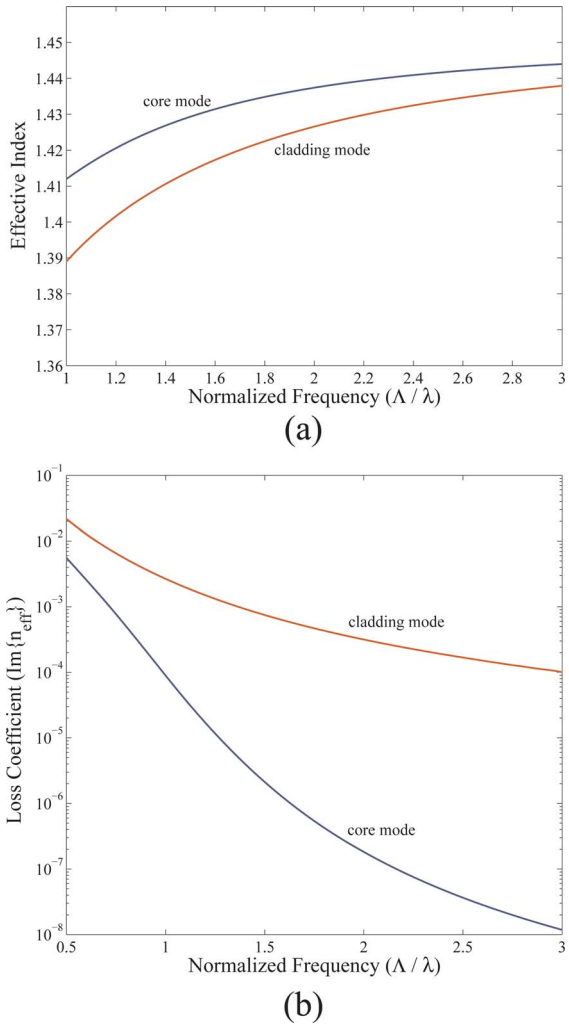

Fig. 2. (Color online) (a) Dispersion curves and (b) losses for the fundamental and the target cladding mode of the fiber shown in Fig. 1 for a symmetrical cladding ($r=r_d=0.2\Lambda$) and for $n_g=1.45$, $n_h=1$. Both modes are double degenerate (x and y polarized).

approximately 10^{-8}, while the cladding mode is apparently much more leaky, with losses several orders of magnitude greater than those of the fundamental mode. Figure 3 shows the optical power of these two modes at $\Lambda/\lambda=2$: the power of the fundamental mode is finely con-

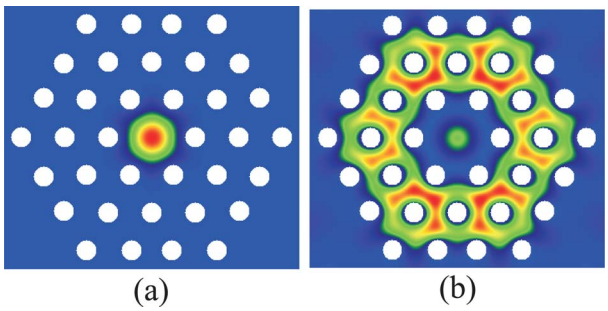

Fig. 3. (Color online) Modal optical power profiles (Poynting vector) for (a) the fundamental and (b) the target cladding mode of the fiber shown in Fig. 1 at $\Lambda/\lambda=2$, $r_d=r=0.2\Lambda$, $n_g=1.45$, and $n_h=1$. The fundamental mode is well confined in the fiber's core, while the power of the cladding mode is split between the core and the region between the first two rings of cylinders of the periodic cladding.

centrated in the defect core, while that of the cladding mode is mainly between the first and the second ring of cylinders in the cladding. It should be noted, however, that a part of the modal power of the cladding mode is also confined in the core, spatially overlapping with the power of the fundamental mode. The loss coefficient here reported translates into actual propagation losses (decibels per meter) via the expression

$$\alpha(\mathrm{dB/m}) = 8.686(2\pi/\lambda)\mathrm{Im}\{n_{\mathrm{eff}}\}. \quad (1)$$

Therefore, losses for the fundamental mode in the case examined remain below 0.05 dB/cm for $\Lambda/\lambda > 2$, assuming an operation wavelength $\lambda = 1.55$ μm.

In order to induce the desired birefringence, we increase the radii r_d of the two defect cylinders of Fig. 1 to the value of $r_d = 0.5\Lambda$. The resulting values of modal birefringence (defined as the difference between the effective indices of the y- and x-polarized modes) for the fundamental mode are shown in Fig. 4, and they agree well with similar structures studied in the literature [35,36]. Birefringence values of up to 10^{-3} can be easily obtained for the fundamental mode; on the other hand, a similar analysis demonstrated that the birefringence corresponding to the various sets of cladding modes overall remains at lower values by 1 order of magnitude. This is because the fiber's symmetry is more significantly perturbed in the core region than in the cladding. Thus, it is the guided mode that is more affected and, therefore, exhibits higher values of modal birefringence.

3. POLARIZING PROPERTIES OF LPGS IN NONINFILTRATED PCFS

Before investigating the effect of inscribing LPGs in the proposed type of birefringent PCFs, we fix the structural parameters of the fiber presented in Fig. 1 to $r = 0.2\Lambda$, r_d

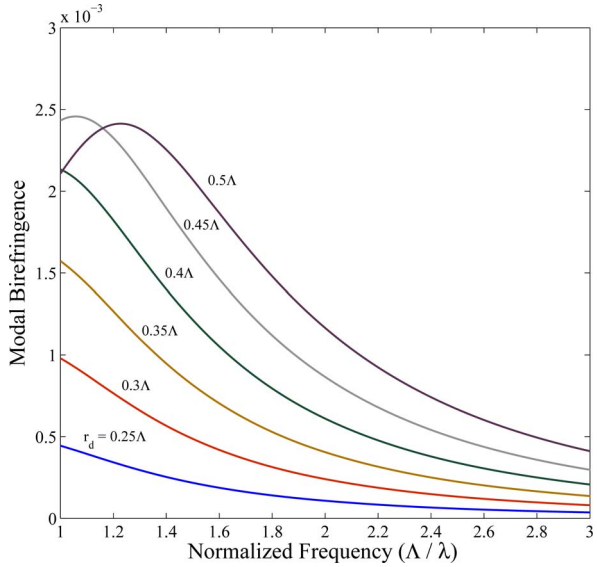

Fig. 4. (Color online) Birefringence curves for the fundamental mode of the fiber shown in Fig. 1 for values of the defect radius ranging from $r_d = 0.25\Lambda$ to $r_d = 0.5\Lambda$. The cladding capillary radius is set to $r = 0.2\Lambda$, the fiberglass is silica $n_g = 1.45$, and the capillaries are not infiltrated ($n_h = 1$). Birefringence values of more than 10^{-3} are predicted in a broad wavelength window.

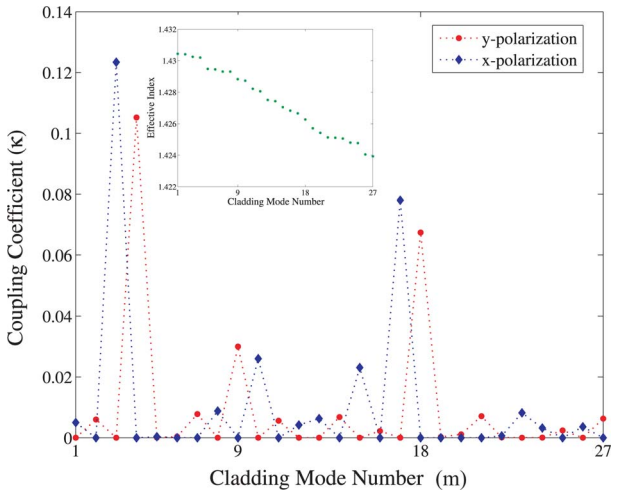

Fig. 5. (Color online) Coupling coefficients between the x-polarized (diamonds) and y-polarized (circles) fundamental mode and the first 27 cladding modes supported by the fiber. Coupling is maximized between pairs of modes with both the same polarization and the same class of symmetry. Inset, effective indices of the cladding modes.

$= 0.5\Lambda$, $n_h = 1$, $\Lambda = 4.4$ μm; this particular set of parameters is typical of commercially available PCFs [37]. Given that the lattice pitch Λ is fixed, the effect of material dispersion of silica (fiberglass) is also consistently taken into account, according to Sellmeier's formula [33].

In order to provide an estimate of the coupling efficiency between the fundamental and the various cladding modes, we initially calculate the effective indices and the modal profiles for the fundamental and the first 27 cladding modes at the indicative wavelength of $\lambda = 1.55$ μm. Afterwards, all modal power profiles are normalized according to the following condition [38]:

$$\int\int_{\infty} \mathbf{E}_{\mathrm{core}}(x,y)\cdot\mathbf{E}^{*}_{\mathrm{core}}(x,y)\mathrm{d}x\mathrm{d}y = \int\int_{\infty} \mathbf{E}_{\mathrm{clad},m}(x,y)\cdot\mathbf{E}^{*}_{\mathrm{clad},m}(x,y)\mathrm{d}x\mathrm{d}y = 1, \quad (2)$$

where $\mathbf{E}$ refers to the transverse electric field of either the core or the cladding modes. Finally, we calculate the coupling coefficients

$$\kappa(m) = \int\int_{\mathrm{core}} \mathbf{E}_{\mathrm{core}}(x,y)\cdot\mathbf{E}^{*}_{\mathrm{clad},m}(x,y)\mathrm{d}x\mathrm{d}y \quad (3)$$

for all pairs between fundamental and cladding modes and for both polarizations of the fundamental mode. The overlap integrals of Eq. (3) are calculated over the cross section of the fiber's core, that is, a region defined by a circle with radius $r = \Lambda$ centered on the fiber's axis, excluding the areas corresponding to the microstructured air holes, where no modulation of the refractive index may be induced. This selection is apparently valid for gratings inscribed in a photosensitive core either in conventional or microstructured fibers; it may not be exactly accurate in LPG-PCFs where the grating is inscribed by other techniques, e.g., mechanical pressure or arc fusion, since in these cases the exact form of the modulation of the refrac-

tive index cannot be accurately predicted. Nevertheless, the results obtained by Eq. (3) do provide a qualitative estimate of the relative coupling efficiency among various pairs of fundamental and cladding modes.

Figure 5 shows the calculated coupling coefficients $\kappa(m)$ corresponding to both the x-polarized (diamonds) and the y-polarized (circles) fundamental mode. It is observed that most pairs of modes yield negligible values of κ; such values correspond either to the coupling between the x- (or y-) polarized fundamental and a y- (or x-) polarized cladding mode, or to the coupling between modes of the same dominant (x- or y-) field component, which, however, belong to different classes of symmetry. The values of κ obtain notable values only in the case of the coupling between fundamental and cladding modes that both exhibit the same polarization, and, in addition, belong to the same class of symmetry. Both core and cladding modes have been sorted following the four symmetry classes according to the C_{2v} classification of McIsaac [31] (the irreducible sector of the studied structure is $[0,\pi/2]$); the x-polarized fundamental mode belongs to the third class, and the y-polarized one to the fourth.

Based on the results regarding the coupling coefficients, we select to study the dispersive properties of the two orthogonal states of polarization for the fundamental and the pair of target cladding modes that ensure maximum coupling efficiency ($m=3,4$ in Fig. 5) in the wavelength regime $1.3\ \mu\text{m}<\lambda<1.8\ \mu\text{m}$. Figure 6 shows the E_y component of the electric field at $\lambda=1.55\ \mu$m for the y-polarized fundamental and the target cladding mode. The part of the optical power of the cladding mode that is confined between the defect capillaries is mostly responsible for the coupling to the fundamental mode.

Having calculated the dispersion curves of the four modes under study (a pair corresponding to each of the two polarizations for both the fundamental and the target cladding mode), we assume that a LPG of period Λ_{LPG} is inscribed in the birefringent PCF. The coupling condition between the fundamental and the cladding mode, which yields the resonant wavelengths, is given by

$$(n_{\text{eff}}^{\text{fund},i}-n_{\text{eff}}^{\text{clad},i})\Lambda_{\text{LPG}}=\lambda_{\text{res}}, \tag{4}$$

where n_{eff} is the effective index of the mode, the index $i=x,y$ refers to the type of polarization, and λ_{res} denotes

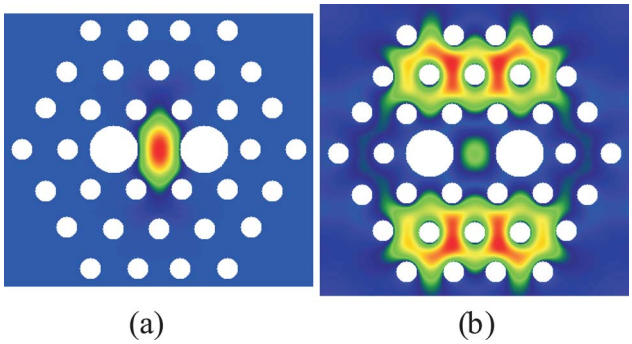

Fig. 6. (Color online) Electric field intensity profiles for the y-polarized fundamental and target cladding modes of the fiber shown at Fig. 1 for $\Lambda=4.4\ \mu$m, $\lambda=1.55\ \mu$m, $n_h=1$, $r=0.2\Lambda$ and $r_d=0.5\Lambda$: (a) Ey component of the fundamental mode, (b) Ey component of the target cladding mode. Silica dispersion has been taken into account.

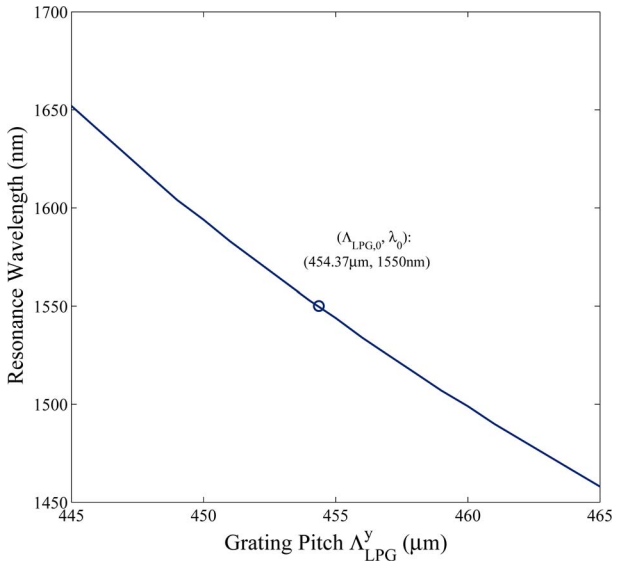

Fig. 7. (Color online) Sensitivity of the y-resonance wavelength over the grating pitch value Λ^y_{LPG}. The average slope of the sensitivity curve is approximately -10 nm/μm.

the resonant wavelengths. Let us assume that we are aiming at the suppression of the propagation of x-polarized light by inducing coupling between the corresponding x-polarized fundamental and cladding modes (X coupling) at an operational wavelength of $\lambda_0=1.55\ \mu$m. The LPG period should be fixed so that the following matching condition is met:

$$\Delta n_x\Lambda_{\text{LPG}}=\lambda_0, \tag{5}$$

where Δn_x is the difference between the effective indices of the x-polarized fundamental and target cladding mode ($\Delta n_x=n_{\text{eff}}^{\text{fund},x}-n_{\text{eff}}^{\text{clad},x}$), which in the case under study yields the value 2.895×10^{-3} at $\lambda_0=1.55\ \mu$m. The value resulting for the LPG period is accordingly $\Lambda^x_{\text{LPG}}=535.44\ \mu$m. The same procedure is followed in the case of designing the

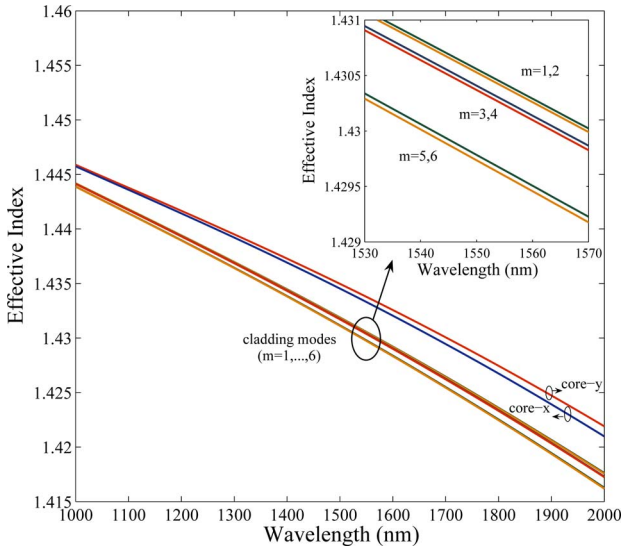

Fig. 8. (Color online) Modal dispersion curves for both polarizations of the fundamental mode and the first six cladding modes ($m=1,\ldots,6$ with respect to Fig. 5) in the wavelength window $1\ \mu\text{m}<\lambda<2\ \mu$m.

LPG to induce Y coupling at $\lambda_0 = 1.55\ \mu$m. The corresponding difference Δn_y equals 3.411×10^{-3}, and the LPG period is calculated to be $\Lambda^y_{\mathrm{LPG}} = 454.37\ \mu$m.

As the calculated LPG pitch values (Λ^x_{LPG}, Λ^y_{LPG}) that set the resonance wavelength exactly at 1.55 μm might not necessarily be achieved in practice, we have also calculated the dependence of the resonant wavelength over the pitch value for the indicative case of Y coupling. Figure 7 reveals an almost linear relation with a sensitivity of approximately -10 nm/μm. For a LPG inscribed via exposure to CO_2 laser pulses, the exact pitch value depends mainly on the accuracy of the positioning stage; typical values for micropositioning stages used for LPG inscription are 0.1 μm [39], which implies that the resonant wavelength may be adjusted within an accuracy of $\sim$1 nm. This value might be further improved by at least 1 order of magnitude if a nanopositioning stage based on piezoelectric elements were used.

Figure 5 shows that the effective index of the next pair of cladding modes that yields substantial values for κ ($m = 9, 10$) is significantly lower than for the target one ($m = 3, 4$). This implies that the resonances corresponding to the coupling between the fundamental mode and the ($m = 9, 10$) pair of cladding modes are expected to lie beyond the wavelength regime of interest. Nevertheless, power coupling phenomena with lower-order cladding modes might also be strong, despite the small values of κ, as the cladding modes exhibit extremely high values of losses. In order to investigate the existence of such resonances around $\lambda_0 = 1.55\ \mu$m, we have extended the modal dispersive analysis in the wavelength range $1\ \mu\mathrm{m} < \lambda < 2\ \mu$m for the pair of core modes and the first six cladding modes ($m = 1, \ldots, 6$); the resulting dispersion curves are shown in Fig. 8.

The resonant wavelengths indicating coupling between either the x- or the y-polarized core mode and the six cladding modes should be given by the nullification of the test functions

$$f^i_{\mathrm{ct}}(\lambda) = [n^{\mathrm{fund},i}_{\mathrm{eff}}(\lambda) - n^{\mathrm{clad},i}_{\mathrm{eff},m}(\lambda)]\Lambda^i_{\mathrm{LPG}} - \lambda \qquad (6)$$

for $i = x, y$ and $m = 1, \ldots, 6$. The results obtained by Eq. (6) are summarized in Table 1, when the grating pitch equals either Λ^x_{LPG} or Λ^y_{LPG}, for both X and Y coupling (the letter X or Y referring to the polarization of the core mode that couples to any cladding mode m). Dashes denote that no resonances were found for $1\ \mu\mathrm{m} < \lambda < 2\ \mu$m. It can be observed that in both cases the predicted resonances corresponding to the polarization that is aimed to be preserved (namely, the results of columns 4 and 5 of Table 1) are located at least 100 nm away from the central wavelength $\lambda_0 = 1.55\ \mu$m.

4. TUNABLE POLARIZING PROPERTIES OF LPGS IN LIQUID-INFILTRATED PCFS

The analysis of LPG-PCFs is extended in the present section targeting the design of thermally tunable all-fiber polarization elements. Thermally tunable properties in a different context have already been demonstrated in LPG-PCFs via the infiltration of PCFs with polymers [40], isotropic fluids [41,42], or nematic liquid crystalline materials [43]. We keep the same parameters as in Section 3, but we now assume that all cladding capillaries of the PCF are infiltrated with a typical isotropic optical liquid [44], which has a thermo-optic coefficient of $-4 \times 10^{-4}/^\circ$C, and its refractive index equals $n_h = 1.33$ at a temperature of 20 °C.

To begin with, we calculate the dispersion curves for each one of the four modes of interest for a total variation of the liquid's refractive index ranging from $n_h = 1.33$ (at 20 °C) to $n_h = 1.3$ (at 95 °C), along the lines of the analysis followed in Section 3. Figure 9 shows a family of curves corresponding to the effective index of the fundamental x-polarized mode and its dependence on the infiltrated liquid's index n_h. As n_h obtains higher values, the difference between the core–cladding indices is suppressed, leading to higher values of effective indices. This behavior is general and applies to the cladding modes as well. In order to track the resonant wavelengths and their dependance on the liquid's refractive index (and consequently the thermal tuning capacity of the LPG-PCF), we calculate the coupling test functions

$$f^i_{\mathrm{ct}}(\lambda, n_h) = [n^{\mathrm{fund},i}_{\mathrm{eff}}(\lambda, n_h) - n^{\mathrm{clad},i}_{\mathrm{eff}}(\lambda, n_h)]\Lambda_{\mathrm{LPG}} - \lambda \qquad (7)$$

for both polarizations ($i = x, y$), and a set of fixed values for Λ_{LPG}, and we search for their nulls in the two-dimensional space (λ, n_h) under examination.

Figure 10 shows the results regarding the tuning efficiency of the investigated design of LPG-PCFs for various values of Λ_{LPG}. The resonant wavelength curves for both

Table 1. LPG Resonances between the Core and the First Six Cladding Modes ($m = 1, \ldots, 6$) in the Wavelength Window $1\ \mu\mathrm{m} < \lambda < 2\ \mu$m

			$\Lambda_{\mathrm{LPG}} \equiv \Lambda^x_{\mathrm{LPG}} = 535.44\ \mu$m		$\Lambda_{\mathrm{LPG}} \equiv \Lambda^y_{\mathrm{LPG}} = 454.37\ \mu$m	
m	Class[a]	DFC[b]	X coupling (nm)	Y coupling (nm)	X coupling (nm)	Y coupling (nm)
1	2	x	—	1194	—	—
2	1	y	—	1179	—	—
3	3	x	1550	1121	—	1605
4	4	y	1441	1102	—	1550
5	2	x	1011	—	1412	1159
6	1	y	—	—	1369	1143

[a]Refers to the modal symmetry class according to McIsaac's C_{2v} classification [31].

[b]Refers to the modal dominant field component; modes of symmetry classes 3 and 4 are fully x and y polarized, respectively.

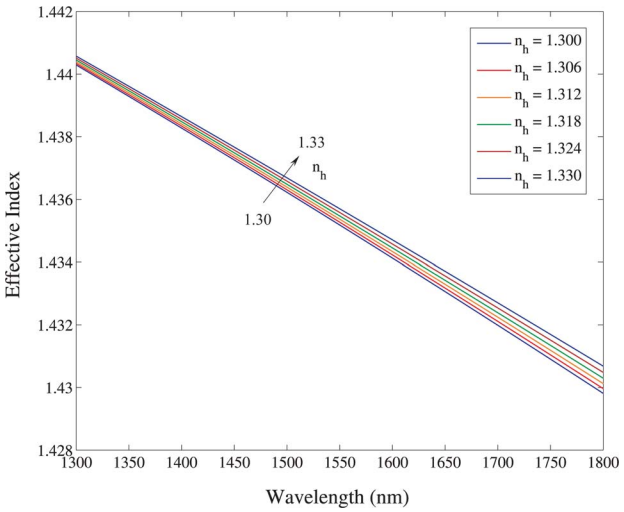

Fig. 9. (Color online) Dependence of the effective index of the x-polarized fundamental mode on the variation of the infiltrated liquid's refractive index n_h. Higher values of n_h lead to an increase of the modal effective index.

X and Y coupling show a paraboliclike behavior with an enhanced tuning efficiency of up to more than 10 nm/°C in the parts of the tuning curves that present maximum slope. The enhanced tuning efficiency originates from the fact that the effect of even small differences in the modal index values, induced by the thermally variable refractive index of the infiltrated liquid, is amplified as the difference $\Delta n_i(\lambda, n_h)$ is multiplied by the LPG period. Although the thermal variation of the refractive index of silica has been neglected, it is not expected to notably modify the results, since silica's thermal coefficient is more than 1 order of magnitude lower than that of the optical liquid [45]; indeed, typical values reported [24,26] for the thermal sensitivity of LPG resonances in noninfiltrated PCFs remain around or below 10 pm/°C, which is negligible compared with the values here reported for the infiltrated PCF.

Despite the general parabolic form of the tuning curves of Fig. 10, there are also extensive regimes where the tuning behavior is almost linear; in these wavelength windows the proposed design allows both linear behavior and an enhanced tuning response. The parabolic shape of the tuning curves may be attributed to the fact that for the specific set of parameters of the example studied, the PCF operates near, or inside, the cutoff regime of the fiber [29]. This is due to the infiltration with the optical liquid, which reduces the effective radius of the capillaries, in contrast to the noninfiltrated case presented in Section 3. The modal dispersion curves of the PCF exhibit a high slope around cutoff, and this behavior is also transferred to the tuning curves of Fig. 10, as test functions (7) are composed by the difference between the function $f_1^i = \Delta n_i(\lambda, n_h)\Lambda_{\mathrm{LPG}}$, which behaves in a similar manner around cutoff, and the linear function $f_2 = \lambda$.

Figure 11 shows the loss coefficient calculated for the x-polarized fundamental mode for a PCF with $\Lambda = 4.4$ μm, $r_d = 0.5\Lambda$, and $n_h = 1.3$, for various values of the cladding hole radius r. It can be deduced that for $r = 0.2\Lambda$, which is the case for the structure studied so far, the losses for the infiltrated PCF obtain values of a few decibels per centi-

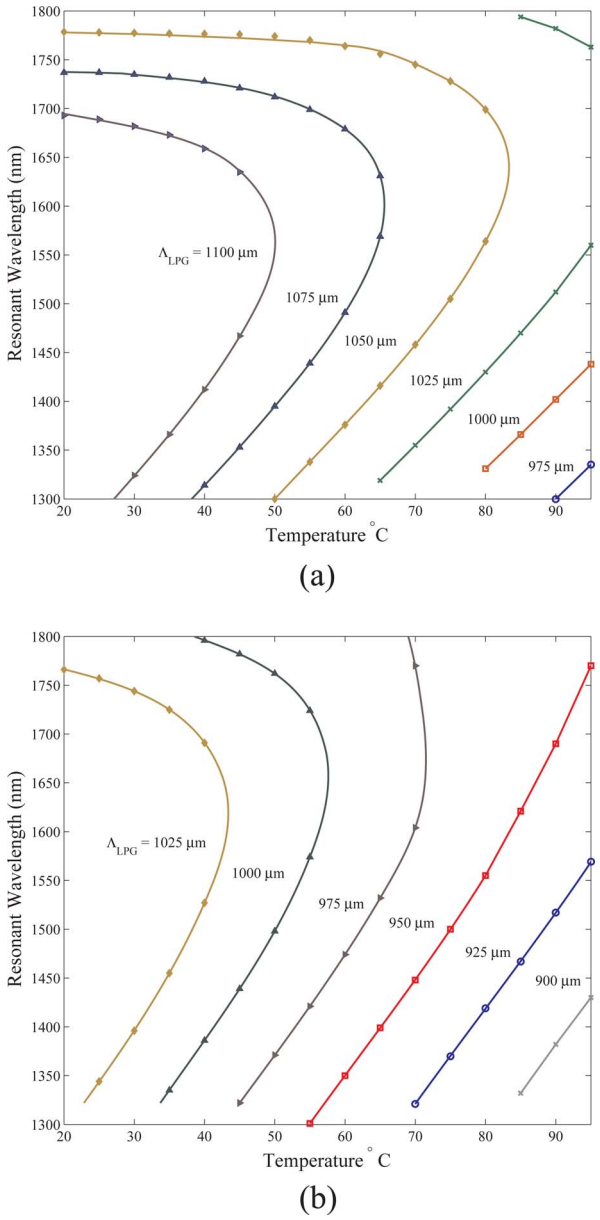

Fig. 10. (Color online) Tuning of the resonant wavelengths for the liquid-infiltrated LPG-PCF under study, as extracted after the calculation of the two-dimensional test function maps $f_{\mathrm{ct}}^i(\lambda, n_h)$: (a) Tuning curves corresponding to X coupling (x-core mode with $m = 3$ cladding mode) and (b) to Y coupling (y-core mode with $m = 4$ cladding mode). Extensive tuning performance (up to >10 nm/°C) is predicted for both X and Y coupling. The tuning curves may be adjusted by properly selecting the period Λ_{LPG} of the grating.

meter in the wavelength window of interest. As the radius obtains higher values, and, subsequently, the fiber's operation moves away from cutoff, losses are highly suppressed. Propagation losses for the fundamental mode drop below 0.1 and 10^{-4} dB/cm, for $r = 0.25\Lambda$ and $r = 0.3\Lambda$, respectively. In order to assess the efficiency of the proposed device in the case of operating away from cutoff, we have repeated the analysis that yielded the results of Fig. 10 for the same parameters, assuming, though, a different cladding hole radius $r = 0.25\Lambda$, for the indicative case of the x-polarized mode. Figure 12 shows the resulting

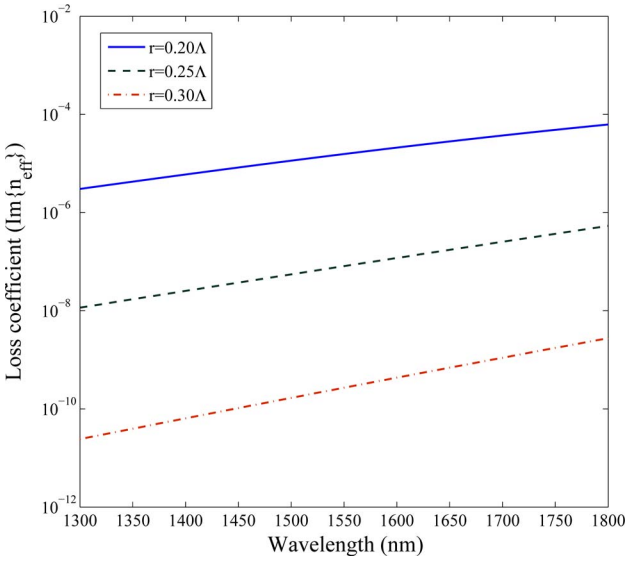

Fig. 11. (Color online) Loss coefficient for the x-polarized mode of a PCF (Fig. 1) with $\Lambda=4.4\ \mu$m, $n_h=1.3$, $r_d=0.5\Lambda$ for different values of the cladding hole radius r.

resonance tuning curves, which are now almost linear, and they do not exhibit the parabolic shape that characterizes the curves of Fig. 10. It could be remarked that lower pitch values are required in order to place the resonances in the desired wavelength window. This is because as the optical liquid covers more space in the cladding, the cladding modal indices decrease notably, while the index of the core mode remains relatively unaffected; thus, the difference between core–cladding effective indices is enhanced, and lower values of Λ_{LPG} are required so that Eq. (7) may be satisfied. Most important, though, the tuning efficiency in the case of $r=0.25\Lambda$ is not drastically undermined, obtaining average values around 6.5 nm/°C, which are comparable with the corresponding linear parts of the curves presented in Fig. 10. These results indicate that extensive tuning efficiency and low propagation losses may be achieved at the same time along the lines of the LPG-PCF polarizing devices here proposed.

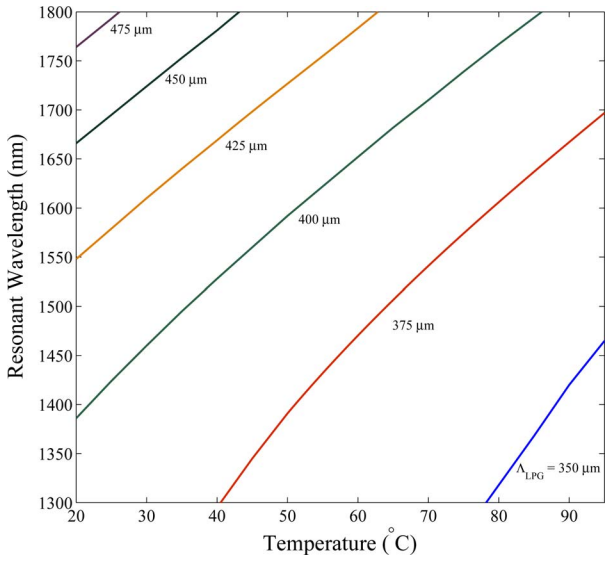

Fig. 12. (Color online) Resonant wavelength tuning curves of the LPG-PCF of Fig. 1 corresponding to the x-polarized mode for $r=0.25\Lambda$ (other parameters as in Fig. 10).

5. CONCLUSIONS

The design of all-fiber polarizing elements based on the inscription of LPGs in PCFs has been numerically investigated for a typical birefringent PCF. It is shown that the resonance wavelengths corresponding to the coupling of the two orthogonal polarizations between the fundamental and a target cladding mode that ensures optimum coupling efficiency may be amply isolated. Furthermore, such LPG-PCFs are also addressed as possible candidates for thermally tunable polarizing operation; results demonstrate that by proper design the resonant wavelengths of liquid-infiltrated birefringent LPG-PCFs may exhibit a paraboliclike response with extensive tuning performance (more than 10 nm/°C) or linear behavior with an enhanced tuning sensitivity of ~6.5 nm/°C.

ACKNOWLEDGMENTS

This work was supported by the Greek General Secretariat of Research and Technology under grant PENED/03ED936.

REFERENCES

1. J. C. Knight, "Photonic crystal fibres," Nature **424**, 847–851 (2003).
2. A. Bjarklev, J. Broeng, and A. S. Bjarklev, *Photonic Crystal Fibers* (Kluwer, 2003).
3. T. A. Birks, J. C. Knight, and P. St. Russell, "Endlessly single-mode photonic crystal fiber," Opt. Lett. **22**, 961–963 (1997).
4. A. Ferrando, E. Silvestre, P. Andrés, J. J. Miret, and M. V. Andres, "Designing the properties of dispersion-flattened photonic crystal fibers," Opt. Express **9**, 687–697 (2001).
5. W. H. Reeves, J. C. Knight, P. St. Russell, and P. J. Roberts, "Demonstration of ultra-flattened dispersion in photonic crystal fibers," Opt. Express **10**, 609–613 (2002).
6. J. C. Knight, T. A. Birks, R. F. Cregan, P. St. Russell, and J. P. de Sandro, "Large mode area photonic crystal fibre," Electron. Lett. **34**, 1347–1348 (1998).
7. K. P. Hansen, "Dispersion flattened hybrid-core nonlinear photonic crystal fiber," Opt. Express **11**, 1503–1509 (2003).
8. C. Kerbage, P. Steinvurzel, P. Reyes, P. S. Westbrook, R. S. Windeler, A. Hale, and B. J. Eggleton, "Highly tunable birefringent microstructured optical fiber," Opt. Lett. **27**, 842–844 (2002).
9. R. Zhang, J. Teipel, and H. Giessen, "Theoretical design of a liquid-core photonic crystal fiber for supercontinuum generation," Opt. Express **14**, 6800–6812 (2006).
10. T. T. Larsen, A. Bjarklev, D. S. Hermann, and J. Broeng, "Optical devices based on liquid crystal photonic bandgap fibres," Opt. Express **11**, 2589–2596 (2003).
11. T. R. Woliński, K. Szaniawska, S. Ertman, P. Lesiak, A. W. Domański, R. Dąbrowski, E. Nowinowski-Kruszelnicki, and J. Wójcik, "Influence of temperature and electrical fields on propagation properties of photonic liquid-crystal fibers," Meas. Sci. Technol. **17**, 985–991 (2006).
12. D. C. Zografopoulos, E. E. Kriezis, and T. D. Tsiboukis, "Photonic crystal-liquid crystal fibers for single-polarization or high-birefringence guidance," Opt. Express **14**, 914–925 (2006).
13. D. C. Zografopoulos, E. E. Kriezis, and T. D. Tsiboukis, "Tunable highly birefringent bandgap-guiding liquid-crystal microstructured fibers," J. Lightwave Technol. **44**, 3427–3432 (2006).

14. A. M. Vengsarkar, P. J. Lemaire, J. B. Judkins, V. Bhatia, T. Erdogan, and J. E. Sipe, "Long-period fiber gratings as band-rejection filters," J. Lightwave Technol. **14**, 58–65 (1996).
15. J. R. Qian and H. F. Chen, "Gain flattening fibre filters using phase-shifted long period fibre gratings," Electron. Lett. **34**, 1132–1133 (1998).
16. A. S. Kurkov, M. Douay, O. Duhem, B. Leleu, J. F. Henninot, J. F. Bayon, and L. Rivoallan, "Long-period fibre gratings as a wavelength selective polarisation element," Electron. Lett. **33**, 616–617 (1997).
17. B. Ortega, L. Dong, W. F. Liu, J. P. de Sandro, L. Reekie, S. I. Tsypina, V. N. Bagratashvili, and R. I. Laming, "High-performance optical fiber polarizers based on long-period gratings in birefringent optical fibers," IEEE Photon. Technol. Lett. **9**, 1370–1372 (1997).
18. J. K. Bae, S. H. Kim, J. H. Kim, J. Bae, S. B. Lee, and J. M. Jeong, "Spectral shape tunable band-rejection filter using a long-period fiber grating with divided coil heaters," IEEE Photon. Technol. Lett. **15**, 407–409 (2003).
19. D. B. Stegall and T. Erdogan, "Dispersion control with use of long-period fiber gratings," J. Opt. Soc. Am. A **17**, 304–312 (2000).
20. A. D. Kersey, M. A. Davis, H. J. Patrick, M. LeBlanc, K. P. Koo, C. G. Askins, M. A. Putnam, and E. J. Friebele, "Fiber grating sensors," J. Lightwave Technol. **15**, 1442–1463 (1997).
21. S. W. James and R. P. Tatam, "Optical fibre long-period grating sensors: characteristics and application," Meas. Sci. Technol. **14**, R49–R61 (2003).
22. B. J. Eggleton, P. S. Westbrook, R. S. Windeler, S. Spalter, and T. A. Strasser, "Grating resonances in air-silica microstructured optical fibers," Opt. Lett. **24**, 1460–1462 (1999).
23. G. Kakarantzas, T. A. Birks, and P. St. Russell, "Structural long-period gratings in photonic crystal fibers," Opt. Lett. **27**, 1013–1015 (2002).
24. H. Dobb, K. Kalli, and D. J. Webb, "Temperature-insensitive long period grating sensors in photonic crystal fiber," Electron. Lett. **40**, 657–658 (2004).
25. J. H. Lim, K. S. Lee, J. C. Kim, B. H. Lee, "Tunable fiber gratings fabricated in photonic crystal fiber by use of mechanical pressure," Opt. Lett. **29**, 331–333 (2004).
26. Y. P. Wang, L. M. Xiao, D. N. Wang, and W. Jin, "In-fiber polarizer based on a long-period fiber grating written on photonic crystal fiber," Opt. Lett. **32**, 1035–1037 (2007).
27. N. A. Mortensen, J. R. Folkenberg, M. D. Nielsen, and K. P. Hansen, "Modal cutoff and the V parameter in photonic crystal fibers," Opt. Lett. **28**, 1879–1881 (2003).
28. G. Renversez, F. Bordas, and B. T. Kuhlmey, "Second mode transition in microstructured optical fibers: determination of the critical geometrical parameter and study of the matrix refractive index and effects of cladding size," Opt. Lett. **30**, 1264–1267 (2005).
29. B. T. Kuhlmey, R. C. McPhedran, C. M. de Sterke, P. A. Robinson, G. Renversez, and D. Maystre, "Microstructured optical fibers: where's the edge?" Opt. Express **10**, 1285–1290 (2002).
30. B. T. Kuhlmey, H. C. Nguyen, M. J. Steel, and B. J. Eggleton, "Confinement loss in adiabatic photonic crystal fiber tapers," J. Opt. Soc. Am. B **23**, 1965–1974 (2006).
31. P. R. McIsaac, "Symmetry-induced modal characteristics of uniform waveguides—I: summary of results," IEEE Trans. Microwave Theory Tech. **MTT-23**, 421–429 (1975).
32. T. P. White, B. T. Kuhlmey, R. C. McPhedran, D. Maystre, G. Renversez, C. M. de Sterke, and L. C. Botten, "Multipole method for microstructured optical fibers. I. Formulation," J. Opt. Soc. Am. B **19**, 2322–2330 (2002).
33. B. T. Kuhlmey, T. P. White, G. Renversez, D. Maystre, L. C. Botten, C. M. de Sterke, and R. C. McPhedran, "Multipole method for microstructured optical fibers. II. Implementation," J. Opt. Soc. Am. B **19**, 2331–2340 (2002).
34. CUDOS Microstructured Optical Fiber Utilities package, http://www.physics.usyd.edu.au/cudos/mofsoftware.
35. K. Suzuki, H. Kubota, S. Kawanishi, M. Tanaka, and M. Fujita, "Optical properties of a low-loss polarization-maintaining photonic crystal fiber," Opt. Express **9**, 676–680 (2001).
36. M. Szpulak, J. Olszewski, T. Martynkien, W. Urbańczyk, and J. Wójcik, "Polarizing photonic crystal fibers with wide operation range," Opt. Commun. **239**, 91–97 (2004).
37. PM-1550-01, Polarisation Maintaining PCF by Blaze Photonics, http://blazephotonics.com.
38. B. J. Eggleton, P. S. Westbrook, C. A. White, C. Kerbage, R. S. Windeler, and G. L. Burdge, "Cladding-mode-resonances in air-silica microstructure optical fibers," J. Lightwave Technol. **18**, 1084–1100 (2000).
39. D. D. Davis, T. K. Gaylord, E. N. Glytsis, S. G. Kosinski, S. C. Mettler, and A. M. Vengsarkar, "Long-period fibre grating fabrication with focused CO_2 laser pulses," Electron. Lett. **34**, 302–303 (1998).
40. P. S. Westbrook, B. J. Eggleton, R. S. Windeler, A. Hale, T. A. Strasser, and G. L. Burdge, "Cladding-mode resonances in hybrid polymer-silica microstructured optical fiber gratings," IEEE Photon. Technol. Lett. **12**, 495–497 (2000).
41. P. Steinvurzel, E. D. Moore, E. C. Magi, and B. J. Eggleton, "Tuning properties of long period gratings in photonic bandgap fibers," Opt. Lett. **31**, 2103–2105 (2006).
42. L. Rindorf, J. B. Jensen, M. Dufva, L. H. Pedersen, P. E. Høiby, and O. Bang, "Photonic crystal fiber long-period gratings for biochemical sensing," Opt. Express **14**, 8224–8231 (2006).
43. D. Noordegraaf, L. Scolari, J. Lægsgaard, L. Rindorf, and T. T. Alkeskjold, "Electrically and mechanically induced long period gratings in liquid crystal photonic bandgap fibers," Opt. Express **15**, 7901–7912 (2007).
44. Cargille Labs, http://cargille.com.
45. G. B. Hocker, "Fiber-optic sensing of pressure and temperature," Appl. Opt. **18**, 1445–1448 (1979).